Blockade of SARS-CoV-2 infection in vitro by highly potent PI3K-α/mTOR/BRD4 inhibitor

Authors: Arpan Acharya[1], Kabita Pandey[1], Michellie Thurman[1], Kishore B. Challagundala[2], Kendra R. Vann[3], Tatiana G. Kutateladze[3], Guillermo A Morales[4], Donald L. Durden*[4,5,6], Siddappa N. Byrareddy*[1,2,7].

Affiliations:

[1]Department of Pharmacology and Experimental Neuroscience, University of Nebraska Medical Center; Omaha, NE 68131, USA.

[2]Department of Biochemistry and Molecular Biology, University of Nebraska Medical Centre, Omaha, NE, 68131, USA

[3]Department of Pharmacology, University of Colorado School of Medicine; Aurora, CO 80045, USA.

[4]SignalRx Pharmaceuticals, Inc.; Cumming, GA 30041, USA.

[5]Division of Pediatric Hematology-Oncology, Department of Pediatrics, Moores Cancer Center, UC San Diego School of Medicine; La Jolla, CA 92130, USA.

[6]Levine Cancer Institute; Charlotte, NC 28204, USA.

[7] Department of Genetics, Cell Biology, and Anatomy, University of Nebraska Medical Centre, Omaha, NE, 68131, USA.

*Corresponding authors.

Email: sid.byrareddy@unmc.edu; ddurden@uscd.edu

One Sentence Summary: Evidence of *in silico* designed chemotype (SF2523) targeting PI3K-α/mTOR/BRD4 inhibits SARS-CoV-2 infection and is highly synergistic with remdesivir.

Abstract:

Pathogenic viruses like SARS-CoV-2 and HIV hijack the host molecular machinery to establish infection and survival in infected cells. This has led the scientific community to explore the molecular mechanisms by which SARS-CoV-2 infects host cells, establishes productive infection, and causes life-threatening pathophysiology. Very few targeted therapeutics for COVID-19 currently exist, such as remdesivir. Recently, a proteomic approach explored the interactions of 26 of 29 SARS-CoV-2 proteins with cellular targets in human cells and identified 67 interactions as potential targets for drug development. Two of the critical targets, the bromodomain and extra-terminal domain proteins (BETs): BRD2/BRD4 and mTOR, are inhibited by the dual inhibitory small molecule SF2523 at nanomolar potency. SF2523 is the only known mTOR PI3K-α/(BRD2/BRD4) inhibitor with potential to block two orthogonal pathways necessary for SARS-CoV-2 pathogenesis in human cells. Our results demonstrate that SF2523 effectively blocks SARS-CoV-2 replication in lung bronchial epithelial cells *in vitro*, showing an IC_{50} value of 1.5 μM, comparable to IC_{50} value of remdesivir (1.1 μM). Further, we demonstrated that the combination of doses of SF2523 and remdesivir is highly synergistic: it allows for the reduction of doses of SF2523 and remdesivir by 25-fold and 4-fold, respectively, to achieve the same potency observed for a single inhibitor. Because SF2523 inhibits two SARS-CoV-2 driven pathogenesis mechanisms involving BRD2/BRD4 and mTOR signaling, our data suggest that SF2523 alone or in combination with remdesivir could be a novel and efficient therapeutic strategy to block SARS-CoV-2 infection and hence be beneficial in preventing severe COVID-19 disease evolution.

INTRODUCTION

Coronavirus disease 2019 (COVID-19) is caused by a novel coronavirus named severe acute respiratory syndrome coronavirus 2 (SARS-CoV-2) (*1*). This is a novel zoonotic single-stranded RNA virus that belongs to the betacoronavirus family, which also includes severe acute respiratory syndrome coronavirus (SARS-CoV) and middle east respiratory syndrome coronavirus (MERS-CoV) (*2*). The ongoing global pandemic of SARS-CoV-2 was first reported from Wuhan, China, in January 2020. As of March 01, 2021, globally, more than 114.30 million confirmed cases and 2.53 million deaths had been reported due to COVID-19 (https://coronavirus.jhu.edu/map.html).

SARS-CoV-2 utilizes host cell angiotensin-converting enzyme 2 (ACE2) as the primary receptor for entry along with several other accessory factors that include TMPRSS2, neuropilin-1, PIKFyve kinase, and CD147, among others (*3*-*8*). After internalization, cathepsin L cleaves the S protein and aids in releasing the viral genome in the host cell cytoplasm (*3*). Inside the cell, virus utilizes the host cell machinery to replicate its positive-sense RNA genome and process the polyproteins to generate functional structural and nonstructural proteins. Then, the viral genome and structural proteins are assembled into progeny viruses, travel to the plasma membrane and are released utilizing lysosomal exocytosis pathways (*9*). During this replication cycle, several viral proteins like NSP1, NSP3, and ORF7a/b suppress the type 1 interferon (IFN) mediated host immune response (*10*), while others activate Toll-like receptors (TLRs) that stimulate the release of proinflammatory cytokines like IL-1β, IL-2, IL-6, IL-7, GCSF, IFN-γ, and TNF-α (*11*).

The pathophysiology of COVID-19 follows a biphasic pattern. In contrast, the initial acute phase of infection is manifested by viral infection-driven symptoms including sore throat, fever, fatigue, dry cough, and/or diarrhea (*12*). In severely ill patients, this is followed by an

72 immunopathologic phase that includes the development of acute respiratory distress syndrome
73 (ARDS), systemic inflammation, and cytokine storm, which is responsible for multiple organ
74 failure and a higher rate of fatalities (*1*). Patients with certain comorbid conditions like
75 hypertension, cardiovascular disease, diabetes, and chronic obstructive pulmonary disorders
76 (COPD) also have a higher probability of developing acute severe respiratory distress syndrome
77 (ARDS). Moreover, a subpopulation of patient's develops neurological disease manifestations
78 like loss of taste and smell, dizziness, confusion, ataxia, seizures and Guillain-Barré Syndrome
79 (GBS) have also been reported (*13*). Among the patients who develop ARDS, many of them
80 succumbed to the disease due to the development of pulmonary fibrosis (*14*). These data suggest
81 that the addition of a currently available or upcoming anti-fibrotic agent for the management of
82 critically ill COVID-19 patients would be beneficial to reduce the rate of fatalities and long-term
83 consequences of pulmonary fibrosis.
84 Although some vaccine candidates received emergency use authorization (EUA) from U.S. Food
85 and Drug Administration (USFDA) to control the rapid spread of the virus, it is anticipated that it
86 will take several months to years to vaccinate the majority of the population (*15*). Again the
87 long-term safety, efficacy, and durability of these vaccines remain unknown specifically for the
88 'special' populations that include children, pregnant women, individuals with comorbid
89 conditions that may impact immune response against a vaccine (*16*). Along with that,
90 preliminary studies indicate that the emerging new strains of SARS-CoV-2 from South Africa
91 having Lys417Asn, Glu484Lys, and Asn501Tyr substitutions in the receptor-binding domain,
92 and Leu18Phe, Asp80Ala, Asp215Gly, 242–244del, and Arg246Ile in the N-terminal domain of
93 spike protein have reduced susceptibility to neutralization by convalescent plasma therapy (*17*).
94 These results question the efficacy of the spike protein-based vaccines against new strains of the

95 virus and further support the fact that this virus will eventually enter an endemic stage with
96 world-wide distribution and high-level mortality. Therefore, other strategies to reduce SARS-
97 CoV-2 and related mutant strain associated morbidity and mortality are urgently needed.
98 These factors underscore the urgent development of an effective therapeutic regimen that will
99 control the rapid spread of the virus and reduce the high rate of fatalities among severely ill
100 patients. From the outset of this pandemic, multiple therapeutic strategies have been tested that
101 are at different stages of development and clinical trials with mixed responses (*18*). The majority
102 of which includes SARS-CoV-2 fusion/entry inhibitors (*19*), RNA-dependent RNA polymerases
103 (RdRps) inhibitors (*20*), viral protease inhibitors (*21*), several classes of immune-suppressive
104 agents to control systemic hyperactive inflammatory response (*22*), and cytokine storm and
105 convalescent plasma treatment (*23*).
106 At present, remdesivir (GS-5734) is the only US FDA-approved antiviral agent in use to treat
107 COVID-19 (*24*). It is a prodrug of a monophosphate nucleotide analog that selectively inhibits
108 RNA-dependent RNA polymerase of SARS-CoV-2 (*25*). A randomized, double-blind, placebo-
109 controlled clinical trial reported shorter hospital stay for patients with COVID-19 when treated
110 with remdesivir than placebo controls (ClinicalTrials.gov: NCT04280705) (*26*). However,
111 another multicenter, randomized clinical trial conducted by WHO did not find any superior effect
112 of remdesivir on hospitalized COVID-19 patients (ClinicalTrials.gov: NCT04315948) (*27*).
113 Therefore, in the absence of a fully effective drug in the prevention of COVID-19, it is warranted
114 to identify and validate more compounds that, individually or in combination with other
115 molecules, will have a profound antiviral efficacy against COVID-19 (*28*).
116 Recently, Gordon et al. (*29*) used a proteomic approach to explore the interactions of 26 out of
117 29 SARS-CoV-2 proteins with cellular targets in human cells and identified 67 potential

118 interactions and targets for drug development. By molecular pathway analysis, they
119 demonstrated an interaction of BRD2/BRD4 with E protein of SARS-CoV-2. In another study
120 Tian et al. using CRISPRi screening shown that BRD2 inhibition down regulate the ACE2
121 expression which block the entry of SARS-CoV-2 within host cells as well as control
122 hyperactive immune response in COVID-19 patients through down regulations of ISGs (*30*).
123 Therefore, they proposed BRD2 as a potential target for development of therapeutics against
124 SARS-CoV-2. Two of the critical host factors responsible for pathogenesis of SARS-CoV-2, the
125 bromodomain and extra-terminal domain proteins (BETs): BRD2/BRD4 and mTOR, are
126 inhibited by the dual inhibitory small molecule SF2523 developed by our group previously. In
127 the present study our *in vitro* data using a human bronchial epithelial cell line (UNCN1T) shows
128 that SF2523 effectively blocks SARS-CoV-2 replication with IC_{50} values comparable to that of
129 remdesivir. We also found that the combination of doses of SF2523 and remdesivir is highly
130 synergistic. There is a 25-fold dose reduction for SF2523 and a 4-fold dose reduction for
131 remdesivir, respectively, when the two compounds are used in combination and they maintain
132 similar potency as a single compound. Future studies in suitable animal models are needed to
133 establish the clinical efficacy of SF2523 alone or a fixed-dose combination of SF2523 and
134 remdesivir as a novel treatment of COVID-19.
135
136 **RESULTS**
137 **Molecular interaction of SF2523 with PI3K-α and BRD4**
138 In a recent study using proteomic analysis, Gordon et al. (*29*) identified 67 host factors that
139 interact with SARS-CoV-2 proteins and represent potential drug development targets. Two of the
140 potential host targets identified, BETs BRD2/BRD4 and mTOR, are inhibited by SF2523.

141 Molecular modeling and structural analysis of predicted molecular interactions of dual BET
142 (BRD2/4)/PI3K-mTOR inhibitor SF2523 with the catalytic domain of PI3K-α are displayed in
143 the top panel of **Fig. 1.** The molecular interactions of SF2523 binding to BRD4-BD1 binding
144 pocket were observed from a 1.8 angstrom resolution crystal structure (PDB ID: 5U28) displayed
145 in the bottom panel of **Fig. 1**. In a cell-free system, the binding potential of SF2523 with its
146 potential targets is shown below the bottom panel of **Fig 1.**

147 **Antiviral efficacy of SF2523 and remdesivir**

148 This study evaluates SF2523 and remdesivir (GS-5734) antiviral efficacy against SARS-CoV-2
149 in Vero-STAT1 knockout cells and UNCN1T cells. STAT1 is a transcription factor essential for
150 interferon-mediated host-cell antiviral response. The STAT1 knockout cells are highly
151 susceptible to viral infection due to the absence of cellular antiviral response and used as control
152 for robust viral infection in this study. On the other hand, UNCN1T is a human bronchial
153 epithelial cell line and expected to demonstrate the *in vivo* pathogenesis of SARS-CoV-2 in the
154 lung and serves as a good *in vitro* model for testing efficacy of antiviral compounds against
155 SARS-CoV-2.

156 Both cell types were treated with SF2523 or remdesivir and their IC_{50} values were determined 24
157 hrs, and 48 hrs post-infection. The replication kinetics were determined from the culture
158 supernatant of SARS-CoV-2 infected UNCN1T and Vero-STAT1 knockout cells in the presence
159 of increasing concentrations of SF2523 and remdesivir and are described in **Fig. 2A** and **Fig. 2B**,
160 respectively. Both compounds show a substantial reduction in SARS-CoV-2 viral load 24 hrs
161 post-infection. Based on SARS-CoV-2 viral loads 24 hrs post infection, SF2523 showed
162 potential antiviral activity and inhibited infection in UNCN1T cells with an IC_{50} of 1.52 μM and
163 remdesivir with an IC_{50} of 1.06 μM. In Vero-STAT1 knockout cells, SF2523 has an IC_{50} of 1.02

164 μM and remdesivir has an IC_{50} of 1.03 μM (**Fig. 2C and 2D**). SARS-CoV-2 replication kinetics
165 48 hrs post-infection in SF2523 and remdesivir treated UNCN1T and Vero-STAT1 knockout
166 cells are described in **Fig. S1A** and **Fig. S1B,** respectively. SF2523 and remdesivir have an IC_{50}
167 value of 1.58 μM and 2.75 μM in UNCN1T cells (**Fig. S1C)** and IC_{50} of 3.22 μM and 0.76 μM
168 in Vero-STAT1 knockout cells (**Fig. S1D**), respectively.

169 **Dose-response relationship and synergy of SF2523 with remdesivir**

170 After testing SF2523 and remdesivir separately, we evaluated a series of combinations of doses
171 of SF2523 and remdesivir with concentrations above and below the IC_{50} determined above. In
172 UNCN1T cells at 24 hrs post-infection, we observed the best inhibitory dose combination. An
173 IC_{50} value of 0.62 μM was observed for remdesivir when combined with 0.1 μM SF2523 (**Fig.**
174 **3A**). Vice versa, we saw the inhibition of viral replication at a fixed remdesivir dose of 0.05 μM
175 and an IC_{50} value of 1.21 μM for SF2523. (**Fig. 3B**). The use of multiple drugs with a different
176 modes of action and synergistic effects is a standard for treatment of infectious diseases to
177 increase the overall efficacy of the therapy and reduce dosage of individual drugs while also
178 reducing the toxicity level and the chances of development of drug resistance (*31*).
179 Based on mass action law and the classic model of enzyme-substrate inhibitor interactions, the
180 median-effect equation was proposed by Chou (*32*), which describes the dose-effect relationship
181 as $(Fa/Fu) = (D/Dm)^m$ or $\log(Fa/Fu) = m\log(D) - m\log(Dm)$. Where the slope (m) of the lines
182 signifies the shape (m = 1, >1, and <1 signify hyperbolic, sigmoidal, and flat sigmoidal dose-
183 effect curves, respectively). Fa is defined as percentage inhibition of viral growth at dose D, and
184 Fu is the fraction that remains unaffected (i.e., Fu = 1 - Fa). The antilog of x-intercept, where
185 Fa/Fu = 1 or log(Fa/Fu) = 0, gives the Dm value. [log(Dm)] signifies the potency of the drugs
186 (where Dm stands for median effective dose or IC_{50} concentration: The concentration required to

187 inhibit 50% growth of the virus). By extrapolating the median-effect equation for multiple drugs,
188 Chou and Talalay proposed the combination index (CI) theorem to quantify synergism and
189 antagonism between drug combinations (*33*). Low CI values with increased Fa values indicate
190 superior compatibility and high synergism between drugs combination (based on Chou and
191 Talalay Combination Index Theorem, CI < 1, = 1, and >1 show synergism, additive effect, and
192 antagonism, respectively). A plot of CI values at different fraction affected (Fa) levels referred to
193 as Fa-CI plot or the Chou-Talalay plot.
194 Using CompuSyn, we generated the Median-Effect plot (Chou plot) of remdesivir (red line),
195 SF2523 (blue line), and the fixed-dose combination of remdesivir and SF2523 (green line) for
196 SARS-CoV-2 infected UNCN1T cells 24 hrs post infection as described above (**Fig. 4A**).
197 Analysis of the Median-Effect, where the X-intercept of the lines indicates potency, shows that
198 the combination dose is more potent than the individual doses of the compounds. In contrast, the
199 Chou-Talalay plot (**Fig. 4B**) indicates the synergistic effect of SF2523 and remdesivir. The dose-
200 response percent inhibition matrix of single and combined treatment of remdesivir and SF2523
201 was computed using SynergyFinder v.2 (**Fig. 4C**). The 3-D interaction landscape between
202 remdesivir and SF2523 was calculated based on Loewe additive model using SynergyFinder v.2
203 in SARS-CoV-2 infected UNCN1T cells 24 hrs post-infection (Loewe synergy score 34.88; with
204 most synergistic area score of 40.24) (**Fig 4D**). Synergy maps highlight synergistic and
205 antagonistic dose regions in red and green colors, respectively. Although there is no defined
206 threshold, drug combinations with a synergy scores above -10 is considered likely antagonistic,
207 and a score between -10 to 10 is deemed a possible additive. Any score above 10 is considered
208 synergistic.

209 Similarly, for SARS-CoV-2 infected Vero-STAT1 knockout cells treated with different
210 combination doses of remdesivir and SF2523, the Median-Effect plot (Chou plot) of remdesivir
211 (red line), SF2523 (blue line), and the fixed-dose combination of remdesivir and SF2523 (green
212 line) is described in **Fig. 5A**, the Chou-Talalay plot (**Fig. 5B**) indicates a synergistic effect of
213 SF2523 and remdesivir. The dose-response percent inhibition matrix of single and combined
214 treatment of remdesivir and SF2523 was computed using SynergyFinder v.2 (**Fig. 5C**) and the 3-
215 D interaction landscape between remdesivir and SF2523 was calculated based on a Loewe
216 additive model using SynergyFinder v.2 in SARS-CoV-2 infected UNCN1T cells 24 hrs post-
217 infection (Loewe synergy score -0.20; with most synergistic area score of 7.67) (**Fig. 5D**).

218 **Table 1** indicates the median effective dose of SF2523, remdesivir, and their fixed-dose
219 combinations. Whereas **Table 2** shows the CI values at ED_{50}, ED_{75}, ED_{90}, and ED_{95} in VERO-
220 STAT1 knockout and UNCN1T cells, which suggests a moderate to strong synergistic effect of
221 the drug combinations. In Vero-STAT1 KO cells at Fa 0.5, we obtained a dose reduction index
222 (DRI) of 11.56 for SF2523 and 2.35 for remdesivir, respectively (with Fa for combination 0.452;
223 2.617 for SF2523 and 0.533 for remdesivir). On the other hand, in UNCN1T cells, we obtained a
224 dose reduction index (DRI) of 25.33 for SF2523 and 3.75 for remdesivir, respectively, (with Fa
225 for combination 0.145; 1.836 for SF2523 and 0.272 for remdesivir).

226 **NMR studies involving SF2523 and BRD4**

227 We note that remdesivir does not alter the potency of SF2523 and does not interfere with the
228 binding of SF2523 to BRD4. To confirm this interaction, we performed NMR titration
229 experiments using ^{15}N-labeled BRD4 domains and showed that remdesivir is incapable of
230 binding to either BD1, BD2, or the ET domain of BRD4, as no significant chemical shift
231 perturbations were observed in ^{1}H,^{15}N heteronuclear single quantum coherence (HSQC) spectra

232 of these domains (**Fig. 6**). However, the subsequent addition of SF2523 to the NMR samples of
233 BD1 and BD2 led to large resonance changes, indicating robust binding, and no binding of
234 SF2523 was detected to the ET domain of BRD4.
235

236 **DISCUSSION**

237 Other than remdesivir, a viral RNA-dependent RNA polymerase inhibitor (*34*), there are no
238 confirmed efficacious molecularly targeted therapeutic agents for the treatment of COVID-19.
239 Targeted therapies that exploit host-virus interaction are likely to be least impacted by the
240 emergence of mutated strains of SARS-CoV-2 and produce more robust, durable treatment
241 options. Gordon *et al*. identified two potential targets for SARS-CoV-2 infectivity, including
242 BRD4 and mTOR kinase pathway (*29*). Using an *in vitro* we show that SF2523 is as potent and
243 effective as remdesivir in blocking the SARS-CoV-2 cytotoxicity and infectivity at
244 concentrations that are achievable and efficacious in animal models (*35*). SF2523 is highly
245 selective and the only known dual inhibitor of PI3K-α/mTOR and BRD4 and is currently slated
246 for clinical development. Hence, it is an excellent candidate for further development for systemic
247 and pulmonary delivery for treatment of COVID-19. Importantly, SF2523 and multiple analogs
248 are the product of extensive *in silico* molecular design to engineer chemotypes with dual or triple
249 inhibitory properties against well-chosen synthetic lethality targets like BRD4, PI3K, and mTOR
250 (*36-38*)

251 The ATP catalytic site of PI3K-α is driven by a critical hydrogen-bond interaction with the NH of
252 Val851. The successful interaction of SF2523 as a PI3K inhibitor was designed with this mode of
253 action where the oxygen atom of the morpholine group engages as a hydrogen-bond acceptor with
254 the required NH of Val851. For the docking against PI3K, we initially created a p110-PI3K-α

255 homology model using the crystal structure of human-derived PI3K-γ (PDB ID: 1E7V) where the
256 human PI3K-α protein sequence was superimposed to the PI3K-γ protein sequence. The resulting
257 3D model of PI3K-α was subsequently used for docking of SF2523 where amino acids within a
258 10 Å radius at the ATP binding site were selected. Successful docking of SF2523 was achieved
259 using FlexX, where the optimal bin36ding mode of SF2523 fulfills 2 pharmacophoric
260 requirements, namely, the spatial location of the carbonyl group of SF2523 and a hydrogen-bond
261 interaction between the morpholine group of SF2523 and Val851 (*39*).

262 BRD4 bromodomain 1 (BRD4-BD1) active site recognizes acetylated lysine residues in histones
263 via hydrogen-bond interaction with the NH of the conserved Asn140 residue. This binding site is
264 a hydrophobic cavity that contains structurally conserved water molecules. For the docking of
265 SF2523 against BDR4-BD1, a human-derived BDR4-BD1 crystal structure co-crystallized with
266 small-molecule BRD4 inhibitor JQ1 (PDB ID: 3MXF) was obtained and amino acids within a 6
267 Å radius of JQ1 were selected. Using AutoDock Vina (*40*) and rDock (*41*), SF2523 was predicted
268 to bind, forming a hydrogen-bond interaction between the carbonyl group of SF2523 and the NH
269 of Asn140 and a conserved water molecule. The morpholine group of SF2523 is oriented towards
270 the opening of the binding site (solvent-exposed). The subsequent successful crystallization of
271 SF2523 with BRD4-BD1 (PDB ID: 5U28) confirmed the predicted binding interaction of SF2523
272 and it also revealed that one of the oxygen atoms of the benzodioxane moiety of SF2523 engages
273 in 2 additional hydrogen-bond interactions with BRD4-BD1, one with GLN85 and one with
274 another conserved water molecule (*35*). NMR data from our laboratory confirms interaction
275 between BRD4 BD1 and acetylated lysine with the C terminus of SARS-CoV-2 E protein. Also,
276 as per Zhang et al., other viral proteins have been shown to have functional interaction with BET
277 BRD4 for viral pathogenesis (*42*).

278 From previous experience, it was observed that in patients infected with SARS and MERS, the
279 viral load peaks only after a week of initial reporting of disease symptoms (*43, 44*). Whereas in
280 the case of SARS-CoV-2, similar to influenza, the viral load peaks along with the onset of
281 disease symptoms (*45*). It was reported that for influenza patients with high viral load at the
282 beginning of disease symptoms, combinational antiviral therapy is more effective than
283 monotherapies (*46, 47*). This is mirrored during the initial phase of the COVID-19 pandemic,
284 where multiple combinational therapeutic approaches using several repurposed drugs show mild
285 to moderate efficacy in treating severely ill patients (*48-50*). To extend this combinational
286 therapeutic approach to treat COVID-19 patients *in vitro,* we tested combination treatment of
287 SF2523 and remdesivir as described above. Our findings suggest that this drug combination is
288 highly synergistic in the human bronchial epithelial cell line with 25-fold dose reduction for
289 SF2523 and 4-fold dose reduction for remdesivir while maintaining similar therapeutic efficacy
290 of individual monotherapies. This reduction in remdesivir dose is also expected to reduce the
291 high incidence of adverse effects related to remdesivir monotherapy (*26, 51*).

292 To characterize the molecular basis for SF2523 mediated inhibition of SARS-CoV-2 replication
293 and confirm the synergistic combination of this compound with remdesivir *in vitro*, we used
294 NMR to look at the capacity of these two chemotypes to interact with BRD4-BD1, BRD4-BD2,
295 and BRD4-ET domains. Consistent with the substantial synergy noted with the two agents,
296 remdesivir did not bind to BRD4; however, SF2523 binds to both BD1 and BD2 but not the
297 extra-terminal (ET) domain of BRD4, supporting differential molecular pathways targeted by
298 these chemically distinct chemotypes. BRD2/BRD4 are epigenetic factors whose two N-
299 terminal bromodomains (BDs) bind with acetylated histones and regulate several proteins (*52*).
300 Several observations related to Gordon et al. (*29*) reporting that BRD4 binds to the SARS-CoV-2

301 E protein include: 1) the E protein forms a homopentameric cation-selective channel which is
302 required for viral budding and release from cells, 2) the E protein is a 72-residue viroporin
303 molecule, 3) mutations or deletions within the transmembrane channel attenuate viral
304 pathogenicity (*53*). Data from emerging mutant strains of SARS-CoV-2 strains indicates
305 presence of several variation in the C terminal domain E protein, that may impact its binding
306 with host protein PALS1with altered disease pathogenesis (*54*). BRD2/BRD4 also has a
307 significant role in cell cycle regulation, inflammation, and inhibition of BRD4 by SF2523
308 enhances the innate and adaptive immune response (*37*). Again, BRD4 drives the secretion of IL-
309 6, CXCL8, and IL17A, which leads to the development of idiopathic pulmonary fibrosis and
310 chronic obstructive pulmonary disease (COPD) (*55*). This suggests that BET inhibitors may
311 disrupt the interaction between BRDs and E protein and will have a favorable outcome in
312 treating COVID-19 patients. LARP1, a significant effector of the mTOR pathway, interacts with
313 nucleocapsid protein (N) (*56*). LARP1 knockdown of inhibitors of mTOR inhibits MERS
314 replication and have an immunosuppressive function (*57*). These data suggest potential important
315 interactions between the SARS-CoV-2 virion and the host machinery elements essential for viral
316 pathogenesis. Campbell et al., reported that SF2523 locks HIV replication in human cells via
317 induction of autophagy (*58*). Moreover, Joshi et al. reported that SF2523 has a potential
318 immunostimulatory impact on innate and adaptive T-cell immunity (*37*). Because SF2523
319 effectively targets two crucial elements of SARS-CoV-2 driven pathogenesis, BETs
320 BRD2/BRD4, and mTOR, and because of its immune activation activity, SF2523 can be a
321 potential therapeutic agent to control COVID-19. It can provide significant clinical benefit in
322 preventing profound COVID-19 disease evolution.

323 Our initial efforts to screen the efficacy of SF2523 monotherapy and combinational therapy
324 against SARS-CoV-2 in the 2D-cellular model is an essential step for initial screening of drug
325 like compounds before initiation of pre-clinical studies and commonly used to explore the
326 molecular mechanism of action. Our future studies will reveal their efficacy in pre-clinical
327 animal models of COVID-19. Its synergistic effect will result in a favorable shift in the plasma
328 Cmax/EC_{90} ratio. Ongoing structural studies to elucidate the interaction of SF2523 with host
329 factors and viral targets will clarify mechanisms of efficacy, and potential resistance as the virus
330 continues to undergo mutagenesis and selection during the pandemic. Considering the emerging
331 data on the life cycle and biology of SARS-CoV-2 infection in humans and the rapid emergence
332 of mutant variants resistant to vaccine candidates, we suggest that a combinatorial approach
333 based on one small molecule which inhibits the interaction of multiple viral targets with host
334 factors necessary for viral pathogenesis will be required to control the mortality and morbidity
335 associated with the pandemic and the likely endemic phase of this disease globally.
336
337 In conclusion, our study demonstrates the *in vitro* efficacy of SF2523 as a monotherapy and in
338 combination with remdesivir against SARS-CoV-2 infection. Considering the marked
339 synergistic effect of these two molecules in a wide dose range in *in vitro* assays, we conclude
340 that, SF2523 alone or in combination with remdesivir represents a future therapeutic approach to
341 obviate the severe disease associated with the ongoing pandemic of SARS-CoV-2.
342
343
344
345

346 **MATERIALS AND METHODS**

347 **Study design**

348 In this *in vitro* study using a human bronchial epithelial cell line (UNCN1T) and Vero-STAT1
349 knockout cells, we evaluate the efficacy of SF2523 (PI3K-mTOR/BRD4 inhibitor) as a
350 monotherapy or in combination with remdesivir against SARS-CoV-2. Using NMR, we also
351 screen the interaction between different domains of BRD4 (BD1, BD2, and ET) and
352 SF2523/remdesivir.

353 **Reagents, cell lines**

354 Remdesivir (GS-5734) was obtained from Selleck Chemicals LLC, 14408 W Sylvanfield Drive,
355 Houston, TX 77014 USA. Vero E6 (ATCC® CRL-1586™) and Vero-STAT1 knockout cells
356 (ATCC® CCL-81-VHG™) were cultured in DMEM containing 10% fetal bovine serum, 2 mM
357 L-glutamine, penicillin (100 units/ml), streptomycin (100 units/mL), and 10 mM HEPES.
358 UNCN1T cells (a human bronchial epithelial cell line; Kerafast; cat# ENC011) were cultured
359 using BEGM media (Bronchial Epithelial Cell Growth Medium; Lonza: cat# CC-3170) in FNC
360 (Athena Enzyme Systems; cat# 0407) coated plates. All other molecular biology grade fine
361 chemicals used in the study were purchased from Sigma-Aldrich, St. Louis, MO, USA, unless
362 otherwise mentioned.

363 ***In silico* docking of SF2523 against PI3K-α and BRD4-BD1.**

364 The docking of SF-2523 with PI3K-α is described previously (*39*). *In silico* docking of SF2523
365 against BRD4-BD1 was performed using AutoDock Vina (*40*) and rDock (*41*). Crystal structure
366 of BRD4 (PDB ID 3MXF) was downloaded from the Protein Data Bank (*59*), residues and water
367 molecules within 6 $Å^3$ of JQ1 were kept, hydrogen atoms and charges were added, and SF2523
368 was docked using default parameters. A minimum of 150 docking solutions were recorded and the

369 conformation of SF2523 matching the expected binding mode (NH of Asn140 forming a hydrogen
370 bond with the carbonyl group of SF2523) with the strongest predicted binding energy was selected.

371 **Protein expression and purification**

372 The pGEX6P-BRD4 BD1 (amino acids 43-180) and pGEX4T-1 BRD4 BD2 (amino acids 342-
373 460) plasmids were expressed in Escherichia coli BL21 (DE3) RIL cells grown in M9 minimal
374 media supplemented with $^{15}NH_4Cl$ and purified as previously described (*35*). The bacteria cells
375 were harvested by centrifugation, resuspended in 10 mM HEPES pH 7.5, 150 mM NaCl, 1 mM
376 TCEP supplemented with DNase I and lysed by sonication. The BRD4 BD1 and BD2 constructs
377 were purified from the cleared lysate using glutathione Sepharose 4B beads and the GST tag was
378 cleaved with PreScission or thrombin protease. The protein was purified using a S100 column
379 (GE Healthcare) equilibrated in 10 mM HEPES pH 7.5, 150 mM NaCl, 1 mM TCEP. BD1
380 protein fractions were assessed for purity (95%) by SDS-PAGE, buffer exchanged into 1X PBS
381 (37 mM NaCl, 2.7 mM KCl, 4.3 mM Na2HPO4, 1.47 mM KH_2PO_4 supplemented with 5 mM
382 DTT and concentrated to ~10-20 mg/mL using 3 kDa Millipore concentrator and stored at -80
383 °C.

384 The pET32a-BRD4 ET domain (amino acids 600-700) vector was obtained from Timothy
385 McKinsey. The N-terminal TRX-6His-S-tagged ET domain was expressed in Escherichia coli
386 Tuner (DE3) competent cells using M9 minimal media supplemented with $^{15}NH_4Cl$. Cells were
387 induced with 0.5 mM IPTG, cultured for 16 h post-induction at 18 °C, and harvested at 5000
388 rpm. The His-tagged protein was purified with Nickel-NTA resin (Thermo Scientific) in 20 mM
389 Sodium Phosphate (pH 7.0) buffer, supplemented with 500 mM NaCl, 10 mM imidazole and 2
390 mM BME. The tagged protein was eluted using a 30-300 mM imidazole gradient elution. The
391 eluted protein was buffer exchanged into cleavage buffer containing 20 mM Tris pH 8.0, 50 mM

392 NaCl, 2 mM CaCl2 and the TRX-6His-S-tag was cleaved overnight at RT with enterokinase
393 protease (NEB). The ET domain was further purified using Nickel-NTA resin (Thermo
394 Scientific) to remove the cleaved tag. Size-exclusion chromatography was performed using a
395 Superdex S75 column. The purified protein was buffer exchanged into 20 mM Tris pH 7.0, 100
396 mM NaCl, 5 mM DTT and concentrated to ~10 mg/mL using 3 kDa Millipore concentrator and
397 stored at -80 °C.

398 **NMR Experiments**

399 For BRD4 BD1 or BD2 experiments, samples containing 0.2 mM ^{15}N-labeled BRD4 BD1/BD2
400 in 1X PBS, 5 mM DTT, and 10% D_2O were prepared. For BRD4 ET experiments, samples
401 containing 0.15 mM ^{15}N-labeled BRD4 ET domain in 20 mM Tris pH 7.0, 100 mM NaCl, 5 mM
402 DTT, and 10% D_2O were prepared. Remdesivir (Selleck Chemicals) and SF2523 (SignalRx
403 Pharmaceuticals, Inc.) were dissolved in 100% DMSO. Remdesivir was titrated into each NMR
404 sample up to 5 molar equivalents. Subsequently, SF2523 was added at a 1:2 equivalence. Two-
405 dimensional ^{1}H,^{15}N HSQC spectra were acquired on a 600 MHz Varian spectrometer fitted with
406 a cryogenic probe at 298 K. Spectra were processed with NMRPipe.

407 **Production of SARS-CoV-2 stocks**

408 SARS-CoV-2 isolate USA-WI1/2020 (BEI; cat# NR-52384) was procured from BEI and
409 passaged in Vero-STAT1 knockout cells. The viral titer was determined using plaque assay (*60*).
410 In brief, Vero E6 cells were seeded in 6-well plates. After 24 hrs, cells were washed with sterile
411 1X PBS. The viral stock was serially diluted and added to cells in duplicate with fresh media and
412 the plates were incubated at 37 ˚C for 1 hour with occasional shaking every 15 minutes. Then 2
413 mL of 0.5% agarose in minimal essential media (MEM) containing 5% FBS and antibiotics was
414 added per well. Plates were incubated at 37 ˚C for 72 hours. Then the cells were fixed with 4%

415 paraformaldehyde overnight, followed by the removal of the overlay and then stained with 0.2%
416 crystal violet to visualize plaque forming units (PFU). All assays involving live SARS-CoV-2
417 were performed in University of Nebraska Medical Center (UNMC) BSL-3 core laboratory
418 setting and approved by the University of Nebraska Medical Center institutional Biosafety
419 Committee (IBC) with the approval number 20-05-029-BL3.

420 **Measuring the antiviral potential of SF2523 and remdesivir against SARS-CoV-2:**

421 UNCN1T and Vero-STAT1 knockout cells were seeded in 96-well plates 24 hours before
422 infection at 20,000 cells/well. Different concentrations of SF2523 and remdesivir (100 μM, 10
423 μM, 5 μM, 1 μM, 0.1 μM, 0.01 μM and 0.001 μM) were added to the cells 2 hours before
424 infection. The cells were infected with 0.1 MOI of SARS-CoV-2 using Opti-MEM I reduced
425 serum medium (Thermo Fisher, Cat#31985062) and incubated for 1 hour at 37 °C with 5% CO_2.
426 For positive control, cells were treated with same volume of DMSO equivalent to the volume of
427 drugs added. Mock infected cells received only Opti-MEM I reduced serum medium. At the end
428 of incubation virus inoculum was removed, cells were washed with 1X PBS 3 times and fresh
429 media supplemented with same concentration of drugs was added. Culture supernatant was
430 collected at 24 hrs and 48 hrs post infection. The SARS-CoV-2 viral load was quantified in
431 culture supernatant using RT-QPCR with primer probes targeting E gene of SARS-CoV-2 using
432 PrimeDirect Probe RT-qPCR Mix (TaKaRa Bio USA, Inc) and Applied Biosystems
433 QuantStudio3 real-time PCR system (Applied Biosystems, Waltham, MA, USA) per the
434 manufacturer's instructions. Primers and probes used for SARS-CoV-2 RNA quantification were
435 as follows: E_Sarbeco_F1: 5' – ACAGGTACGTTAATAGTTAATAGCGT – 3' (400 nM),
436 E_Sarbeco_R2: 5' – ATATTGCAGCAGTACGCACACA – 3' (400 nM) and E_Sarbeco_P1: 5'
437 – FAM - ACACTAGCCATCCTTACTGCGCTTCG - BHQ1 – 3' (200 nM) as recommended by

438 WHO. The SARS-CoV-2 genome equivalent copies were calculated using quantitative PCR
439 (qPCR) control RNA from heat-inactivated SARS-CoV-2, isolate USA-WA1/2020 (BEI; cat#
440 NR-52347). The percentage inhibition of SARS-CoV-2 replication in SF2523 and remdesivir
441 treated wells were calculated with respect to viral concentration in positive control wells that
442 were treated with DMSO (considered 0% inhibition) and negative control wells (uninfected
443 cells). IC_{50} values were calculated using four parameter variable slope sigmoidal dose-response
444 models using Graph Pad Prism 8.0 software.

445 **Measuring the combinational antiviral potential of SF2523 and remdesivir**

446 To determine possible combinational antiviral effect of SF2523 and remdesivir against SARS-
447 CoV-2, we tested 5 (remdesivir) X 4 (SF2523) dose combinations in SARS-CoV-2 infected
448 UNCN1T and Vero-STAT1 knockout cells. The percentage inhibition of viral replication for
449 each dose combinations were determined by RT-QPCR as described above. In brief, the
450 UNCN1T and Vero-STAT1 knockout cells were seeded in 96-well plates at a density of 20,000
451 cells/wells 24 hrs before infection. Two hours before infection the cells were treated with
452 different combination doses of SF2523 and remdesivir, infected with 0.1 MOI of SARS-CoV-2.
453 Twenty-four hours post infection culture supernatant was collected and SARS-CoV-2 viral load
454 was quantified using RT-QPCR as described above. The percentage inhibition of SARS-CoV-2
455 replication in the culture supernatant by different combined doses of SF2523 and remdesivir
456 were determined with respect to viral concentration in positive control wells that were treated
457 with DMSO (considered 0% inhibition) and negative control wells (uninfected cells). Then the
458 percent inhibition of viral replication for 1:1 fixed dose combination of the drugs was used to
459 generate CI-Fa, isobologram and dose-response plots. The combination index (CI) was
460 calculated using multiple drug effect equation developed by Chou and Talalay using the

461 CompuSyn algorithm (https://www.combosyn.com). A CI values of <1 indicate synergy, values
462 >1 indicate antagonism, and values equal to 1 indicate additive effects (*31, 33, 61*). Dose-
463 response percent inhibition matrix of single and combined treatment of remdesivir and SF2523
464 in SARS-CoV-2 infected UNCN1T and Vero-STAT1 knockout cells 24 hrs post infection and 3-
465 D interaction landscape between remdesivir and SF2523 were calculated based on Loewe
466 additive model using SynergyFinder v.2 (*62*).

467 **Statistical analysis**

468 IC_{50} values were calculated using four parameter variable slope sigmoidal dose-response models
469 using Graph Pad Prism 8.0 software. The combination index (CI) was calculated using multiple
470 drug effect equation developed by Chou and Talalay using the CompuSyn algorithm
471 (https://www.combosyn.com). 3-D interaction landscape between remdesivir and SF2523 was
472 calculated based on Loewe additive model using SynergyFinder v.2.

473

474 **References:**

475 1. H. A. Rothan, S. N. Byrareddy, The epidemiology and pathogenesis of coronavirus disease
476 (COVID-19) outbreak. *J Autoimmun* **109**, 102433 (2020).
477 2. G. Guo, L. Ye, K. Pan, Y. Chen, D. Xing, K. Yan, Z. Chen, N. Ding, W. Li, H. Huang, L.
478 Zhang, X. Li, X. Xue, New Insights of Emerging SARS-CoV-2: Epidemiology, Etiology,
479 Clinical Features, Clinical Treatment, and Prevention. *Front Cell Dev Biol* **8**, 410 (2020).
480 3. R. K. Suryawanshi, R. Koganti, A. Agelidis, C. D. Patil, D. Shukla, Dysregulation of Cell
481 Signaling by SARS-CoV-2. *Trends Microbiol*, (2020).
482 4. X. Ou, Y. Liu, X. Lei, P. Li, D. Mi, L. Ren, L. Guo, R. Guo, T. Chen, J. Hu, Z. Xiang, Z.
483 Mu, X. Chen, J. Chen, K. Hu, Q. Jin, J. Wang, Z. Qian, Characterization of spike

484 glycoprotein of SARS-CoV-2 on virus entry and its immune cross-reactivity with SARS-
485 CoV. *Nat Commun* **11**, 1620 (2020).
486 5. P. Xia, A. Dubrovska, Tumor markers as an entry for SARS-CoV-2 infection? *FEBS J* **287**,
487 3677-3680 (2020).
488 6. L. Cantuti-Castelvetri, R. Ojha, L. D. Pedro, M. Djannatian, J. Franz, S. Kuivanen, F. van
489 der Meer, K. Kallio, T. Kaya, M. Anastasina, T. Smura, L. Levanov, L. Szirovicza, A.
490 Tobi, H. Kallio-Kokko, P. Osterlund, M. Joensuu, F. A. Meunier, S. J. Butcher, M. S.
491 Winkler, B. Mollenhauer, A. Helenius, O. Gokce, T. Teesalu, J. Hepojoki, O. Vapalahti,
492 C. Stadelmann, G. Balistreri, M. Simons, Neuropilin-1 facilitates SARS-CoV-2 cell entry
493 and infectivity. *Science* **370**, 856-860 (2020).
494 7. J. L. Daly, B. Simonetti, K. Klein, K. E. Chen, M. K. Williamson, C. Anton-Plagaro, D. K.
495 Shoemark, L. Simon-Gracia, M. Bauer, R. Hollandi, U. F. Greber, P. Horvath, R. B.
496 Sessions, A. Helenius, J. A. Hiscox, T. Teesalu, D. A. Matthews, A. D. Davidson, B. M.
497 Collins, P. J. Cullen, Y. Yamauchi, Neuropilin-1 is a host factor for SARS-CoV-2
498 infection. *Science* **370**, 861-865 (2020).
499 8. M. Hoffmann, H. Kleine-Weber, S. Schroeder, N. Kruger, T. Herrler, S. Erichsen, T. S.
500 Schiergens, G. Herrler, N. H. Wu, A. Nitsche, M. A. Muller, C. Drosten, S. Pohlmann,
501 SARS-CoV-2 Cell Entry Depends on ACE2 and TMPRSS2 and Is Blocked by a Clinically
502 Proven Protease Inhibitor. *Cell* **181**, 271-280 e278 (2020).
503 9. S. Ghosh, T. A. Dellibovi-Ragheb, A. Kerviel, E. Pak, Q. Qiu, M. Fisher, P. M. Takvorian,
504 C. Bleck, V. W. Hsu, A. R. Fehr, S. Perlman, S. R. Achar, M. R. Straus, G. R. Whittaker,
505 C. A. M. de Haan, J. Kehrl, G. Altan-Bonnet, N. Altan-Bonnet, beta-Coronaviruses Use

506 Lysosomes for Egress Instead of the Biosynthetic Secretory Pathway. *Cell* **183**, 1520-1535
507 e1514 (2020).
508 10. H. Xia, Z. Cao, X. Xie, X. Zhang, J. Y. Chen, H. Wang, V. D. Menachery, R. Rajsbaum,
509 P. Y. Shi, Evasion of Type I Interferon by SARS-CoV-2. *Cell Rep* **33**, 108234 (2020).
510 11. P. Conti, G. Ronconi, A. Caraffa, C. E. Gallenga, R. Ross, I. Frydas, S. K. Kritas, Induction
511 of pro-inflammatory cytokines (IL-1 and IL-6) and lung inflammation by Coronavirus-19
512 (COVI-19 or SARS-CoV-2): anti-inflammatory strategies. *J Biol Regul Homeost Agents*
513 **34**, 327-331 (2020).
514 12. G. Pascarella, A. Strumia, C. Piliego, F. Bruno, R. Del Buono, F. Costa, S. Scarlata, F. E.
515 Agro, COVID-19 diagnosis and management: a comprehensive review. *J Intern Med* **288**,
516 192-206 (2020).
517 13. A. Acharya, B. D. Kevadiya, H. E. Gendelman, S. N. Byrareddy, SARS-CoV-2 Infection
518 Leads to Neurological Dysfunction. *J Neuroimmune Pharmacol* **15**, 167-173 (2020).
519 14. P. M. George, A. U. Wells, R. G. Jenkins, Pulmonary fibrosis and COVID-19: the potential
520 role for antifibrotic therapy. *Lancet Respir Med* **8**, 807-815 (2020).
521 15. B. M. Prubeta, Current State of the First COVID-19 Vaccines. *Vaccines (Basel)* **9**, (2021).
522 16. M. Connors, B. S. Graham, H. C. Lane, A. S. Fauci, SARS-CoV-2 Vaccines: Much
523 Accomplished, Much to Learn. *Ann Intern Med*, (2021).
524 17. H. Tegally, E. Wilkinson, R. J. Lessells, J. Giandhari, S. Pillay, N. Msomi, K. Mlisana, J.
525 N. Bhiman, A. von Gottberg, S. Walaza, V. Fonseca, M. Allam, A. Ismail, A. J. Glass, S.
526 Engelbrecht, G. Van Zyl, W. Preiser, C. Williamson, F. Petruccione, A. Sigal, I. Gazy, D.
527 Hardie, N. Y. Hsiao, D. Martin, D. York, D. Goedhals, E. J. San, M. Giovanetti, J.

528 Lourenco, L. C. J. Alcantara, T. de Oliveira, Sixteen novel lineages of SARS-CoV-2 in
529 South Africa. *Nat Med*, (2021).
530 18. H. Li, Y. Zhou, M. Zhang, H. Wang, Q. Zhao, J. Liu, Updated Approaches against SARS-
531 CoV-2. *Antimicrob Agents Chemother* **64**, (2020).
532 19. S. Xiu, A. Dick, H. Ju, S. Mirzaie, F. Abdi, S. Cocklin, P. Zhan, X. Liu, Inhibitors of SARS-
533 CoV-2 Entry: Current and Future Opportunities. *J Med Chem* **63**, 12256-12274 (2020).
534 20. R. Pokhrel, P. Chapagain, J. Siltberg-Liberles, Potential RNA-dependent RNA polymerase
535 inhibitors as prospective therapeutics against SARS-CoV-2. *J Med Microbiol* **69**, 864-873
536 (2020).
537 21. B. Luan, T. Huynh, X. Cheng, G. Lan, H. R. Wang, Targeting Proteases for Treating
538 COVID-19. *J Proteome Res* **19**, 4316-4326 (2020).
539 22. A. H. Mansourabadi, M. Sadeghalvad, H. R. Mohammadi-Motlagh, N. Rezaei, The
540 immune system as a target for therapy of SARS-CoV-2: A systematic review of the current
541 immunotherapies for COVID-19. *Life Sci* **258**, 118185 (2020).
542 23. S. T. H. Liu, H. M. Lin, I. Baine, A. Wajnberg, J. P. Gumprecht, F. Rahman, D. Rodriguez,
543 P. Tandon, A. Bassily-Marcus, J. Bander, C. Sanky, A. Dupper, A. Zheng, F. T. Nguyen,
544 F. Amanat, D. Stadlbauer, D. R. Altman, B. K. Chen, F. Krammer, D. R. Mendu, A. Firpo-
545 Betancourt, M. A. Levin, E. Bagiella, A. Casadevall, C. Cordon-Cardo, J. S. Jhang, S. A.
546 Arinsburg, D. L. Reich, J. A. Aberg, N. M. Bouvier, Convalescent plasma treatment of
547 severe COVID-19: a propensity score-matched control study. *Nat Med* **26**, 1708-1713
548 (2020).

549 24. H. X. J. Lin, S. Cho, V. Meyyur Aravamudan, H. Y. Sanda, R. Palraj, J. S. Molton, I.
550 Venkatachalam, Remdesivir in Coronavirus Disease 2019 (COVID-19) treatment: a review
551 of evidence. *Infection*, (2021).
552 25. J. A. Al-Tawfiq, A. H. Al-Homoud, Z. A. Memish, Remdesivir as a possible therapeutic
553 option for the COVID-19. *Travel Med Infect Dis* **34**, 101615 (2020).
554 26. J. H. Beigel, K. M. Tomashek, L. E. Dodd, A. K. Mehta, B. S. Zingman, A. C. Kalil, E.
555 Hohmann, H. Y. Chu, A. Luetkemeyer, S. Kline, D. Lopez de Castilla, R. W. Finberg, K.
556 Dierberg, V. Tapson, L. Hsieh, T. F. Patterson, R. Paredes, D. A. Sweeney, W. R. Short,
557 G. Touloumi, D. C. Lye, N. Ohmagari, M. D. Oh, G. M. Ruiz-Palacios, T. Benfield, G.
558 Fatkenheuer, M. G. Kortepeter, R. L. Atmar, C. B. Creech, J. Lundgren, A. G. Babiker, S.
559 Pett, J. D. Neaton, T. H. Burgess, T. Bonnett, M. Green, M. Makowski, A. Osinusi, S.
560 Nayak, H. C. Lane, A.-S. G. Members, Remdesivir for the Treatment of Covid-19 - Final
561 Report. *N Engl J Med* **383**, 1813-1826 (2020).
562 27. W. H. O. S. T. Consortium, H. Pan, R. Peto, A. M. Henao-Restrepo, M. P. Preziosi, V.
563 Sathiyamoorthy, Q. Abdool Karim, M. M. Alejandria, C. Hernandez Garcia, M. P. Kieny,
564 R. Malekzadeh, S. Murthy, K. S. Reddy, M. Roses Periago, P. Abi Hanna, F. Ader, A. M.
565 Al-Bader, A. Alhasawi, E. Allum, A. Alotaibi, C. A. Alvarez-Moreno, S. Appadoo, A.
566 Asiri, P. Aukrust, A. Barratt-Due, S. Bellani, M. Branca, H. B. C. Cappel-Porter, N.
567 Cerrato, T. S. Chow, N. Como, J. Eustace, P. J. Garcia, S. Godbole, E. Gotuzzo, L.
568 Griskevicius, R. Hamra, M. Hassan, M. Hassany, D. Hutton, I. Irmansyah, L. Jancoriene,
569 J. Kirwan, S. Kumar, P. Lennon, G. Lopardo, P. Lydon, N. Magrini, T. Maguire, S.
570 Manevska, O. Manuel, S. McGinty, M. T. Medina, M. L. Mesa Rubio, M. C. Miranda-
571 Montoya, J. Nel, E. P. Nunes, M. Perola, A. Portoles, M. R. Rasmin, A. Raza, H. Rees, P.

572 P. S. Reges, C. A. Rogers, K. Salami, M. I. Salvadori, N. Sinani, J. A. C. Sterne, M.
573 Stevanovikj, E. Tacconelli, K. A. O. Tikkinen, S. Trelle, H. Zaid, J. A. Rottingen, S.
574 Swaminathan, Repurposed Antiviral Drugs for Covid-19 - Interim WHO Solidarity Trial
575 Results. *N Engl J Med*, (2020).
576 28. A. Pizzorno, B. Padey, J. Dubois, T. Julien, A. Traversier, V. Duliere, P. Brun, B. Lina, M.
577 Rosa-Calatrava, O. Terrier, In vitro evaluation of antiviral activity of single and combined
578 repurposable drugs against SARS-CoV-2. *Antiviral Res* **181**, 104878 (2020).
579 29. D. E. Gordon, G. M. Jang, M. Bouhaddou, J. Xu, K. Obernier, K. M. White, M. J. O'Meara,
580 V. V. Rezelj, J. Z. Guo, D. L. Swaney, T. A. Tummino, R. Huttenhain, R. M. Kaake, A. L.
581 Richards, B. Tutuncuoglu, H. Foussard, J. Batra, K. Haas, M. Modak, M. Kim, P. Haas, B.
582 J. Polacco, H. Braberg, J. M. Fabius, M. Eckhardt, M. Soucheray, M. J. Bennett, M. Cakir,
583 M. J. McGregor, Q. Li, B. Meyer, F. Roesch, T. Vallet, A. Mac Kain, L. Miorin, E. Moreno,
584 Z. Z. C. Naing, Y. Zhou, S. Peng, Y. Shi, Z. Zhang, W. Shen, I. T. Kirby, J. E. Melnyk, J.
585 S. Chorba, K. Lou, S. A. Dai, I. Barrio-Hernandez, D. Memon, C. Hernandez-Armenta, J.
586 Lyu, C. J. P. Mathy, T. Perica, K. B. Pilla, S. J. Ganesan, D. J. Saltzberg, R. Rakesh, X.
587 Liu, S. B. Rosenthal, L. Calviello, S. Venkataramanan, J. Liboy-Lugo, Y. Lin, X. P. Huang,
588 Y. Liu, S. A. Wankowicz, M. Bohn, M. Safari, F. S. Ugur, C. Koh, N. S. Savar, Q. D. Tran,
589 D. Shengjuler, S. J. Fletcher, M. C. O'Neal, Y. Cai, J. C. J. Chang, D. J. Broadhurst, S.
590 Klippsten, P. P. Sharp, N. A. Wenzell, D. Kuzuoglu-Ozturk, H. Y. Wang, R. Trenker, J.
591 M. Young, D. A. Cavero, J. Hiatt, T. L. Roth, U. Rathore, A. Subramanian, J. Noack, M.
592 Hubert, R. M. Stroud, A. D. Frankel, O. S. Rosenberg, K. A. Verba, D. A. Agard, M. Ott,
593 M. Emerman, N. Jura, M. von Zastrow, E. Verdin, A. Ashworth, O. Schwartz, C. d'Enfert,
594 S. Mukherjee, M. Jacobson, H. S. Malik, D. G. Fujimori, T. Ideker, C. S. Craik, S. N. Floor,

595 J. S. Fraser, J. D. Gross, A. Sali, B. L. Roth, D. Ruggero, J. Taunton, T. Kortemme, P.
596 Beltrao, M. Vignuzzi, A. Garcia-Sastre, K. M. Shokat, B. K. Shoichet, N. J. Krogan, A
597 SARS-CoV-2 protein interaction map reveals targets for drug repurposing. *Nature* **583**,
598 459-468 (2020).
599 30. R. Tian, A. J. Samelson, V. V. Rezelj, M. Chen, G. N. Ramadoss, X. Guo, A. M. Kain, Q.
600 D. Tran, S. A. Lim, I. Lui, J. Nunez, S. J. Rockwood, N. Liu, J. Carlson-Stevermer, J. Oki,
601 T. Maures, K. Holden, J. S. Weissman, J. A. Wells, B. Conklin, M. Vignuzzi, M.
602 Kampmann, BRD2 inhibition blocks SARS-CoV-2 infection in vitro by reducing
603 transcription of the host cell receptor ACE2. *bioRxiv*, (2021).
604 31. T. C. Chou, Theoretical basis, experimental design, and computerized simulation of
605 synergism and antagonism in drug combination studies. *Pharmacol Rev* **58**, 621-681
606 (2006).
607 32. T. C. Chou, Derivation and properties of Michaelis-Menten type and Hill type equations
608 for reference ligands. *J Theor Biol* **59**, 253-276 (1976).
609 33. T. C. Chou, P. Talalay, Quantitative analysis of dose-effect relationships: the combined
610 effects of multiple drugs or enzyme inhibitors. *Adv Enzyme Regul* **22**, 27-55 (1984).
611 34. R. T. Eastman, J. S. Roth, K. R. Brimacombe, A. Simeonov, M. Shen, S. Patnaik, M. D.
612 Hall, Remdesivir: A Review of Its Discovery and Development Leading to Emergency Use
613 Authorization for Treatment of COVID-19. *ACS Cent Sci* **6**, 672-683 (2020).
614 35. F. H. Andrews, A. R. Singh, S. Joshi, C. A. Smith, G. A. Morales, J. R. Garlich, D. L.
615 Durden, T. G. Kutateladze, Dual-activity PI3K-BRD4 inhibitor for the orthogonal
616 inhibition of MYC to block tumor growth and metastasis. *Proc Natl Acad Sci U S A* **114**,
617 E1072-E1080 (2017).

618 36. L. Carlino, G. Rastelli, Dual Kinase-Bromodomain Inhibitors in Anticancer Drug
619 Discovery: A Structural and Pharmacological Perspective. *J Med Chem* **59**, 9305-9320
620 (2016).
621 37. S. Joshi, A. R. Singh, K. X. Liu, T. V. Pham, M. Zulcic, D. Skola, H. B. Chun, C. K. Glass,
622 G. A. Morales, J. R. Garlich, D. L. Durden, SF2523: Dual PI3K/BRD4 Inhibitor Blocks
623 Tumor Immunosuppression and Promotes Adaptive Immune Responses in Cancer. *Mol*
624 *Cancer Ther* **18**, 1036-1044 (2019).
625 38. H. Zhu, J. H. Mao, Y. Wang, D. H. Gu, X. D. Pan, Y. Shan, B. Zheng, Dual inhibition of
626 BRD4 and PI3K-AKT by SF2523 suppresses human renal cell carcinoma cell growth.
627 *Oncotarget* **8**, 98471-98481 (2017).
628 39. G. A. Morales, J. R. Garlich, J. Su, X. Peng, J. Newblom, K. Weber, D. L. Durden,
629 Synthesis and cancer stem cell-based activity of substituted 5-morpholino-7H-thieno[3,2-
630 b]pyran-7-ones designed as next generation PI3K inhibitors. *J Med Chem* **56**, 1922-1939
631 (2013).
632 40. O. Trott, A. J. Olson, AutoDock Vina: improving the speed and accuracy of docking with
633 a new scoring function, efficient optimization, and multithreading. *J Comput Chem* **31**,
634 455-461 (2010).
635 41. S. Ruiz-Carmona, D. Alvarez-Garcia, N. Foloppe, A. B. Garmendia-Doval, S. Juhos, P.
636 Schmidtke, X. Barril, R. E. Hubbard, S. D. Morley, rDock: a fast, versatile and open source
637 program for docking ligands to proteins and nucleic acids. *PLoS Comput Biol* **10**, e1003571
638 (2014).

639 42. Q. Zhang, L. Zeng, C. Shen, Y. Ju, T. Konuma, C. Zhao, C. R. Vakoc, M. M. Zhou,
640 Structural Mechanism of Transcriptional Regulator NSD3 Recognition by the ET Domain
641 of BRD4. *Structure* **24**, 1201-1208 (2016).
642 43. J. F. Chan, Y. Yao, M. L. Yeung, W. Deng, L. Bao, L. Jia, F. Li, C. Xiao, H. Gao, P. Yu,
643 J. P. Cai, H. Chu, J. Zhou, H. Chen, C. Qin, K. Y. Yuen, Treatment With
644 Lopinavir/Ritonavir or Interferon-beta1b Improves Outcome of MERS-CoV Infection in a
645 Nonhuman Primate Model of Common Marmoset. *J Infect Dis* **212**, 1904-1913 (2015).
646 44. V. C. Cheng, B. S. Tang, A. K. Wu, C. M. Chu, K. Y. Yuen, Medical treatment of viral
647 pneumonia including SARS in immunocompetent adult. *J Infect* **49**, 262-273 (2004).
648 45. K. K. To, O. T. Tsang, W. S. Leung, A. R. Tam, T. C. Wu, D. C. Lung, C. C. Yip, J. P.
649 Cai, J. M. Chan, T. S. Chik, D. P. Lau, C. Y. Choi, L. L. Chen, W. M. Chan, K. H. Chan,
650 J. D. Ip, A. C. Ng, R. W. Poon, C. T. Luo, V. C. Cheng, J. F. Chan, I. F. Hung, Z. Chen,
651 H. Chen, K. Y. Yuen, Temporal profiles of viral load in posterior oropharyngeal saliva
652 samples and serum antibody responses during infection by SARS-CoV-2: an observational
653 cohort study. *Lancet Infect Dis* **20**, 565-574 (2020).
654 46. J. Dunning, J. K. Baillie, B. Cao, F. G. Hayden, R. International Severe Acute, C. Emerging
655 Infection, Antiviral combinations for severe influenza. *Lancet Infect Dis* **14**, 1259-1270
656 (2014).
657 47. I. F. N. Hung, K. K. W. To, J. F. W. Chan, V. C. C. Cheng, K. S. H. Liu, A. Tam, T. C.
658 Chan, A. J. Zhang, P. Li, T. L. Wong, R. Zhang, M. K. S. Cheung, W. Leung, J. Y. N. Lau,
659 M. Fok, H. Chen, K. H. Chan, K. Y. Yuen, Efficacy of Clarithromycin-Naproxen-
660 Oseltamivir Combination in the Treatment of Patients Hospitalized for Influenza A(H3N2)

661 Infection: An Open-label Randomized, Controlled, Phase IIb/III Trial. *Chest* **151**, 1069-
662 1080 (2017).
663 48. C. R. Rayner, L. Dron, J. J. H. Park, E. H. Decloedt, M. F. Cotton, V. Niranjan, P. F. Smith,
664 M. G. Dodds, F. Brown, G. Reis, D. Wesche, E. J. Mills, Accelerating Clinical Evaluation
665 of Repurposed Combination Therapies for COVID-19. *Am J Trop Med Hyg* **103**, 1364-
666 1366 (2020).
667 49. I. F. Hung, K. C. Lung, E. Y. Tso, R. Liu, T. W. Chung, M. Y. Chu, Y. Y. Ng, J. Lo, J.
668 Chan, A. R. Tam, H. P. Shum, V. Chan, A. K. Wu, K. M. Sin, W. S. Leung, W. L. Law,
669 D. C. Lung, S. Sin, P. Yeung, C. C. Yip, R. R. Zhang, A. Y. Fung, E. Y. Yan, K. H. Leung,
670 J. D. Ip, A. W. Chu, W. M. Chan, A. C. Ng, R. Lee, K. Fung, A. Yeung, T. C. Wu, J. W.
671 Chan, W. W. Yan, W. M. Chan, J. F. Chan, A. K. Lie, O. T. Tsang, V. C. Cheng, T. L.
672 Que, C. S. Lau, K. H. Chan, K. K. To, K. Y. Yuen, Triple combination of interferon beta-
673 1b, lopinavir-ritonavir, and ribavirin in the treatment of patients admitted to hospital with
674 COVID-19: an open-label, randomised, phase 2 trial. *Lancet* **395**, 1695-1704 (2020).
675 50. P. K. Panda, A. Bandyopadhyay, B. C. Singh, B. Moirangthem, G. Chikara, S. Saha, Y. A.
676 Bahurupi, Safety and efficacy of antiviral combination therapy in symptomatic patients of
677 Covid-19 infection - a randomised controlled trial (SEV-COVID Trial): A structured
678 summary of a study protocol for a randomized controlled trial. *Trials* **21**, 866 (2020).
679 51. Q. Fan, B. Zhang, J. Ma, S. Zhang, Safety profile of the antiviral drug remdesivir: An
680 update. *Biomed Pharmacother* **130**, 110532 (2020).
681 52. Q. Niu, Z. Liu, E. Alamer, X. Fan, H. Chen, J. Endsley, B. B. Gelman, B. Tian, J. H. Kim,
682 N. L. Michael, M. L. Robb, J. Ananworanich, J. Zhou, H. Hu, Structure-guided drug design

683 identifies a BRD4-selective small molecule that suppresses HIV. *J Clin Invest* **129**, 3361-
684 3373 (2019).
685 53. V. S. Mandala, M. J. McKay, A. A. Shcherbakov, A. J. Dregni, A. Kolocouris, M. Hong,
686 Structure and drug binding of the SARS-CoV-2 envelope protein transmembrane domain
687 in lipid bilayers. *Nat Struct Mol Biol* **27**, 1202-1208 (2020).
688 54. M. S. Rahman, M. N. Hoque, M. R. Islam, I. Islam, I. D. Mishu, M. M. Rahaman, M.
689 Sultana, M. A. Hossain, Mutational insights into the envelope protein of SARS-CoV-2.
690 *Gene Rep* **22**, 100997 (2021).
691 55. N. Wang, R. Wu, D. Tang, R. Kang, The BET family in immunity and disease. *Signal*
692 *Transduct Target Ther* **6**, 23 (2021).
693 56. A. Husain, S. N. Byrareddy, Rapamycin as a potential repurpose drug candidate for the
694 treatment of COVID-19. *Chem Biol Interact* **331**, 109282 (2020).
695 57. J. Dyall, R. Gross, J. Kindrachuk, R. F. Johnson, G. G. Olinger, Jr., L. E. Hensley, M. B.
696 Frieman, P. B. Jahrling, Middle East Respiratory Syndrome and Severe Acute Respiratory
697 Syndrome: Current Therapeutic Options and Potential Targets for Novel Therapies. *Drugs*
698 **77**, 1935-1966 (2017).
699 58. G. R. Campbell, R. S. Bruckman, S. D. Herns, S. Joshi, D. L. Durden, S. A. Spector,
700 Induction of autophagy by PI3K/MTOR and PI3K/MTOR/BRD4 inhibitors suppresses
701 HIV-1 replication. *J Biol Chem* **293**, 5808-5820 (2018).
702 59. H. M. Berman, J. Westbrook, Z. Feng, G. Gilliland, T. N. Bhat, H. Weissig, I. N.
703 Shindyalov, P. E. Bourne, The Protein Data Bank. *Nucleic Acids Res* **28**, 235-242 (2000).

704 60. E. J. Mendoza, K. Manguiat, H. Wood, M. Drebot, Two Detailed Plaque Assay Protocols
705 for the Quantification of Infectious SARS-CoV-2. *Curr Protoc Microbiol* **57**, ecpmc105
706 (2020).
707 61. T. C. Chou, Drug combination studies and their synergy quantification using the Chou-
708 Talalay method. *Cancer Res* **70**, 440-446 (2010).
709 62. A. Ianevski, A. K. Giri, T. Aittokallio, SynergyFinder 2.0: visual analytics of multi-drug
710 combination synergies. *Nucleic Acids Res* **48**, W488-W493 (2020).

711 **Acknowledgements:** We acknowledge the UNMC BSL-3 core facility for allowing us to
712 perform all *in vitro* experiments involving SARS-CoV-2. 'The University of Nebraska Medical
713 Center BSL-3 Core Facility is administrated through the Office of the Vice Chancellor for
714 Research and supported by the Nebraska Research Initiative (NRI).' "The following reagent was
715 deposited by the Centers for Disease Control and Prevention and obtained through BEI
716 Resources, NIAID, NIH: (a) SARS-Related Coronavirus 2, Isolate USA-WI1/2020, NR-52384
717 and (b) Quantitative PCR (qPCR) Control RNA from Heat-Inactivated SARS-Related
718 Coronavirus 2, Isolate USA-WA1/2020, NR 52347."
719 **Funding:** This work is partially supported by National Institute of Allergy and Infectious
720 Diseases Grant R01 AI129745, 5P30 CA036727-33 and Frances E. Lageschulte and Evelyn B.
721 Weese New Frontiers in Medical Research Fund to SNB and NIH grants HL151334 and
722 CA252707 to T.G.K; and CA215651 to DLD.

723 **Author contributions:**

724 Conceptualization: DLD, SNB.

725 Methodology: AA, SNB, TGK, SNB.

726 Investigation: AA, KP, MT, KRV

727 Data analysis: AA, KP, MT, KRV, KBC, TGK, DLD, SNB

728 Funding acquisition: SNB

729 Writing – original draft: AA, SNB, DLD, TGK, GAM

730 Writing – review & editing: AA, KP, MT, KBC, KRV, TGK, DLD, SNB, GAM.

731 **Competing interests:** DLD and GMA declare financial interest in SF2523 via their holding in

732 SignalRx Pharmaceuticals, Inc.

733 **Data and materials availability:** All data related with this study are presented in the manuscript

734 or the supplementary materials.

735

736

737

738

739

740

741

742

743

744

745

746

747

748

749

750

751 **Figures**

TOP: PI3K-alpha with SF2523 (docking)

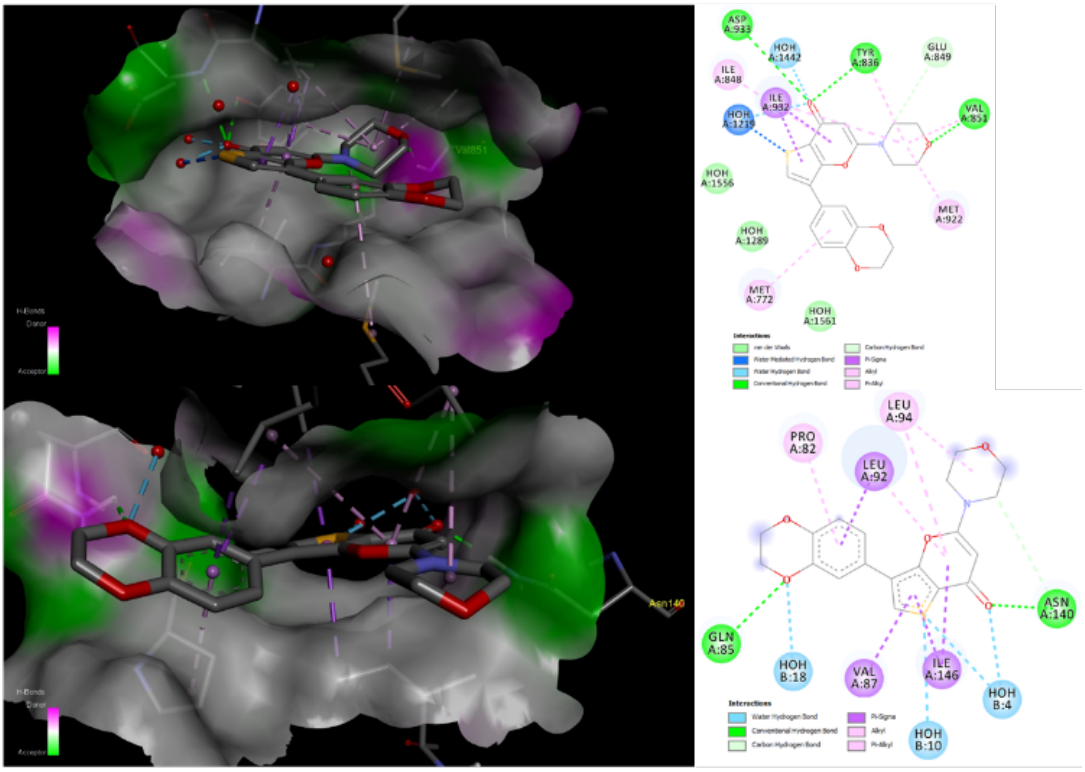

BOTTOM: BRD4-BD1 with SF2523 (xray)

752

BRD2-1*	BRD2-2*	BRD4-1	BRD4-2	PI3Kα	PI3Kβ	PI3Kδ	PI3Kγ	mTor
190	800	79	732	13	214	12	158	280

753 * = Kd (nM)

754 **Fig. 1.** Predicted binding (docking) of SF2523 in PI3K-α catalytic domain (upper panel) and
755 observed binding in crystal structure of SF2523 bound to BRD4-BD1 acetyl lysine binding site
756 (1.8 Angstroms resolution) (bottom panel). *In vitro* (enzymatic) potency of SF2523 against
757 targets.

758

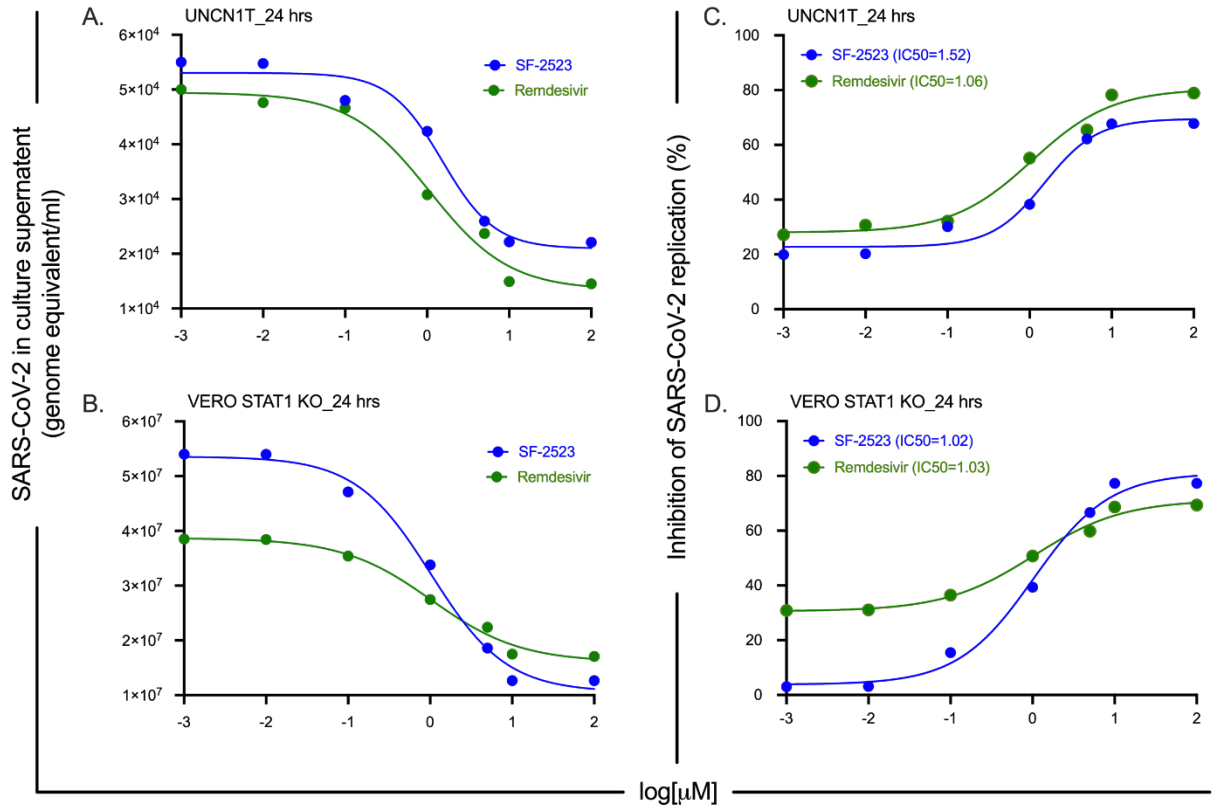

759

760 **Fig 2. SARS-CoV-2 viral loads and dose-response curve in SF2523 and remdesivir treated**
761 **and SARS-CoV-2 infected UNCN1T cells and Vero-STAT1 knockout cells.** (A & B) Real-
762 time quantitative PCR analysis of SARS-CoV-2 genome equivalent per ml of culture supernatant
763 after 24 hrs post-infection in SF2523 (in blue) and remdesivir (in green) treated UNCN1T cells

764 and Vero-STAT1 knockout cells with indicated drug concentrations, respectively. (C & D)
765 SF2523 (in blue) and remdesivir (in green) dose response curve by percentage inhibition of
766 SARS-CoV-2 replication 24 hrs post infection in UNCN1T cells and Vero-STAT1 knockout
767 cells with indicated drug concentrations, respectively.

768

769

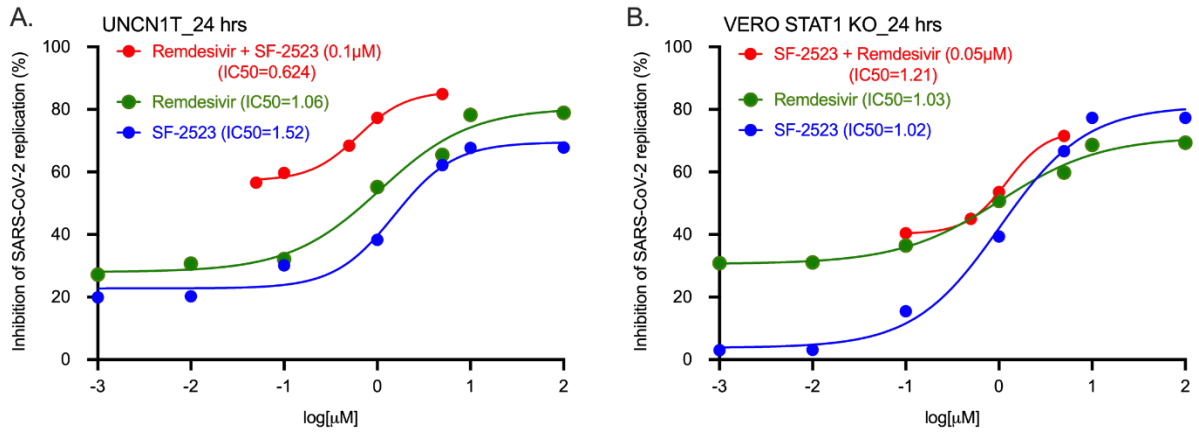

770

771 **Fig 3. Dose-response curve for single and combination of SF2523 and remdesivir in SARS-**
772 **CoV-2 infected UNCN1T cells and Vero-STAT1 knockout cells 24 hrs post infection.** (**A**)
773 Dose response curve of remdesivir (green: IC_{50} = 1.06 μM), (blue: IC_{50} = 1.52 μM), and
774 remdesivir with a fixed dose combination of SF2523 (0.1 μM) (red: IC_{50} = 0.625) by percentage
775 inhibition of SARS-CoV-2 replication 24 hrs post infection in UNCN1T cells; (**B**) Dose response
776 curve of remdesivir (green: IC_{50} = 1.03μM), (blue: IC_{50} = 1.02 μM), and SF2523 with a fixed
777 dose combination of remdesivir (0.05μM) (red: IC_{50} = 1.21) by percentage inhibition of SARS-
778 CoV-2 replication 24 hrs post infection (IC_{50} = 1.02 μM) in Vero-STAT1 knockout cells.

779

780

781

782

783

784

785

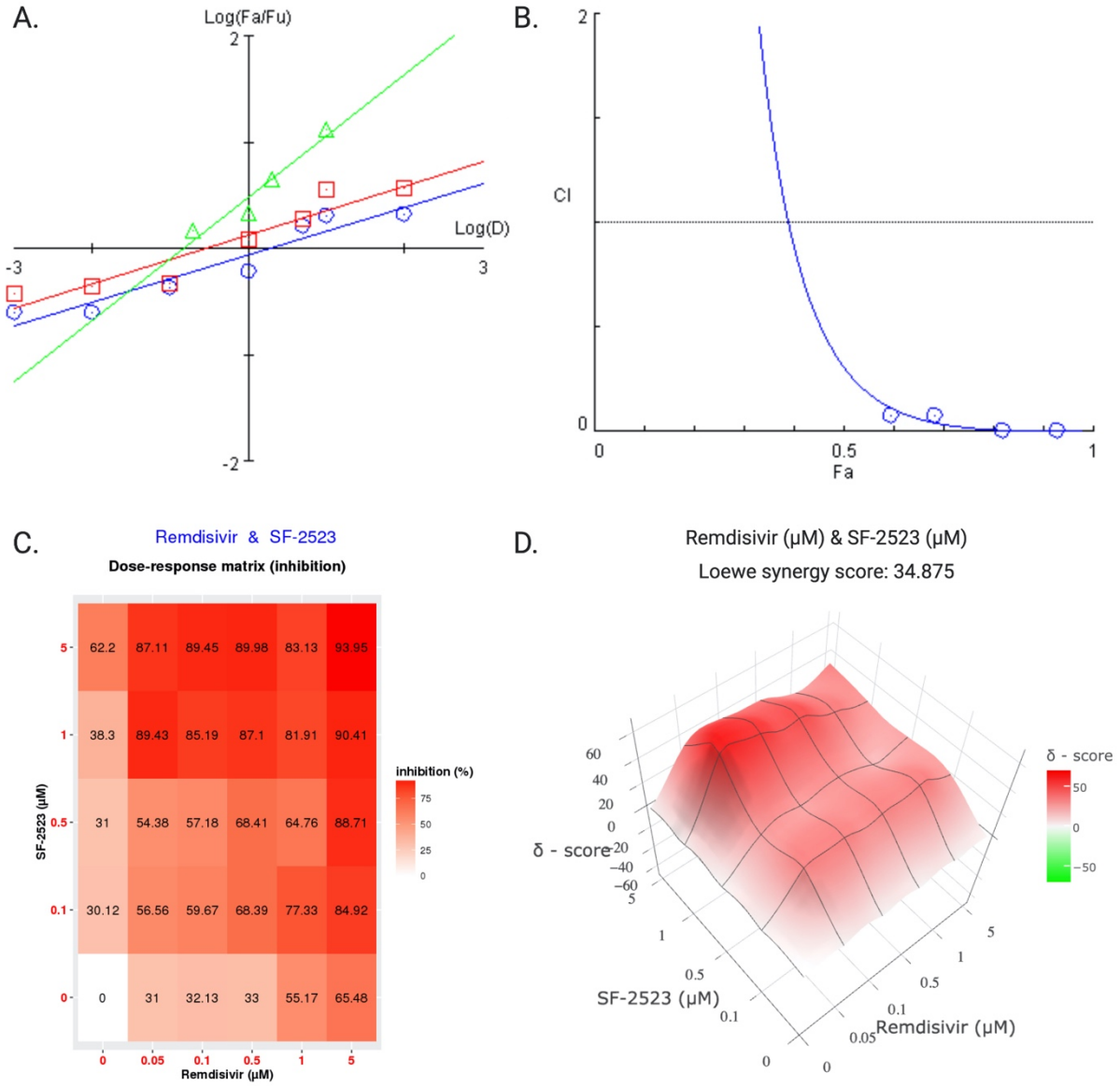

786

787 **Fig 4. Synergistic effect of remdesivir and SF2523 combined treatment against SARS-CoV-**
788 **2 infected UNCN1T cells 24 hrs post infection. (A)** The Median-Effect plot (Chou plot) of
789 remdesivir (the red line with square data points, SF2523 (blue line with circular data points) and
790 fixed dose combination of remdesivir and SF2523 (green line with triangular data points). The
791 median-Effect equation, that describes the dose-effect relationship is given by (Fa/Fu) =
792 $(D/Dm)^m$ or log(Fa/Fu) = m log(D) – m log(Dm). The slope (m) of the lines signifies the shape
793 (m = 1, >1, and <1 signify hyperbolic, sigmoidal, and flat sigmoidal dose-effect curves
794 respectively). Fa is defined as percentage inhibition of viral growth at dose D and Fu is the
795 fraction that remain unaffected (i.e., Fu = 1 - Fa). The antilog of x-intercept, where Fa/Fu = 1 or
796 log(Fa/Fu) = 0, gives the Dm value. [log(Dm)] signifies the potency of the drugs (where Dm
797 stands for median effective dose or IC_{50} concentration: The concentration required to inhibit 50%
798 growth of the virus). (**B**) Combination index plot or Chou-Talaly plot or Fa-CI plot: A plot of CI
799 (combination index) on the Y-axis vs Fa on X-axis for fixed dose combination of remdesivir and
800 SF2523 in SARS-CoV-2 infected UNCN1T cells (blue line with circular data points); Low CI
801 values with increase in Fa values indicates superior compatibility and high synergism between
802 drugs combination (based on Chou and Talalay Combination Index Theorem, CI < 1, = 1, and >1
803 indicate synergism, additive effect, and antagonism, respectively). (**C**) Dose-response percent
804 inhibition matrix of single and combined treatment of remdesivir and SF2523 in SARS-CoV-2
805 infected UNCN1T cells 24 hrs post infection. (**D**) 3-D interaction landscape between remdesivir
806 and SF2523 calculated based on Loewe additive model using SynergyFinder v.2 in SARS-CoV-
807 2 infected UNCN1T cells 24 hrs post infection (Loewe synergy score 34.88; with most
808 synergistic area score of 40.24). Synergy maps highlight synergistic and antagonistic dose
809 regions in red and green colors, respectively. Although there is no defined threshold, for drug

810 combinations with a synergy scores above -10 is considered likely antagonistic, score between -

811 10 to 10 is considered likely additive and score above 10 is considered synergistic.

812

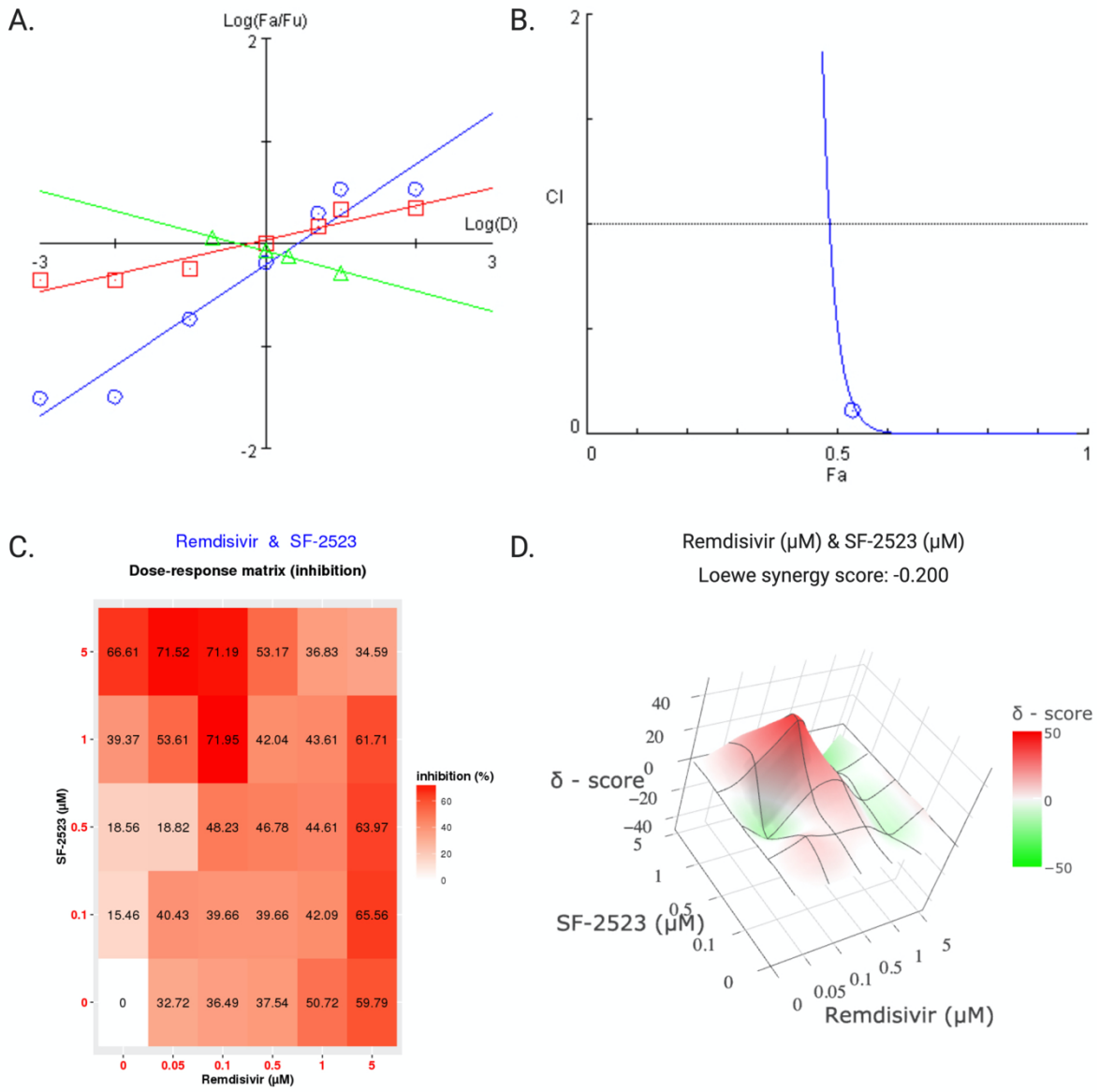

813

814 **Fig 5. Synergistic effect of remdesivir and SF2523 combined treatment against SARS-CoV-**

815 **2 in Vero-STAT1 knockout cells 24 hrs post infection. (A)** The Median-Effect plot (Chou

816 plot) of remdesivir (the red line with square data points, SF2523 (blue line with circular data

817 points) and fixed dose combination of remdesivir and SF2523 (green line with triangular data
818 points). The median-Effect equation, that describes the dose-effect relationship is given by
819 $(Fa/Fu) = (D/Dm)^m$ or $\log(Fa/Fu) = m \log(D) - m \log(Dm)$. The slope (m) of the lines signifies
820 the shape (m = 1, >1, and <1 signify hyperbolic, sigmoidal, and flat sigmoidal dose-effect curves
821 respectively). Fa is defined as percentage inhibition of viral growth at dose D and Fu is the
822 fraction that remain unaffected (i.e., Fu = 1 - Fa). The antilog of x-intercept, where Fa/Fu = 1 or
823 log(Fa/Fu) = 0, gives the Dm value. [log(Dm)] signifies the potency of the drugs (where Dm
824 stands for median effective dose or IC_{50} concentration: The concentration required to inhibit 50%
825 growth of the virus). (**B**) Combination index plot or Chou-Talaly plot or Fa-CI plot: A plot of CI
826 (combination index) on the Y-axis vs Fa on X-axis for fixed dose combination of remdesivir and
827 SF2523 in SARS-CoV-2 infected Vero-STAT1 knockout cells (blue line with circular data
828 points); Low CI values with increase in Fa values indicates superior compatibility and high
829 synergism between drugs combination (based on Chou and Talalay Combination Index Theorem,
830 CI < 1, = 1, and >1 indicate synergism, additive effect, and antagonism, respectively). (**C**) Dose-
831 response percent inhibition matrix of single and combined treatment of remdesivir and SF2523
832 in SARS-CoV-2 infected Vero-STAT1 knockout cells 24 hrs post infection. (**D**) 3-D interaction
833 landscape between remdesivir and SF2523 calculated based on Loewe additive model using
834 SynergyFinder v.2 in SARS-CoV-2 infected Vero-STAT1 knockout cells 24 hrs post infection
835 (Loewe synergy score -0.20; with most synergistic area score of 7.67). Synergy maps highlight
836 synergistic and antagonistic dose regions in red and green colors, respectively. Although there is
837 no defined threshold, for drug combinations with a synergy scores above -10 is considered likely
838 antagonistic, score between -10 to 10 is considered likely additive and score above 10 is
839 considered synergistic.

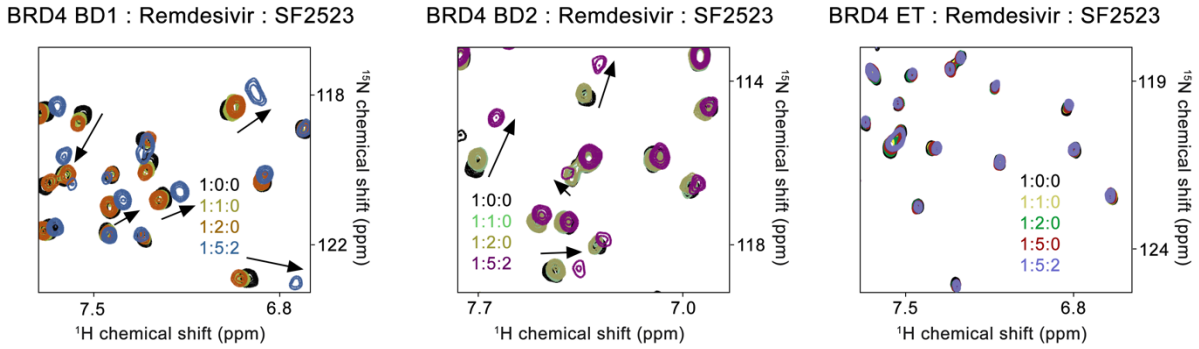

Fig 6. Remdesivir does not bind to the BRD4 BD domains and does not affect binding of SF2523 to BDs. Superimposed ^{1}H,^{15}N HSQC spectra of uniformly ^{15}N-labeled BD1 (left), BD2 (middle) and ET (right) domains of BRD4 with the indicated ligands added in a stepwise manner. The spectra are color coded according to the protein:ligand ratios. Small resonance changes are due to weak binding of DMSO, which was confirmed by titrating DMSO alone to separate samples of these domains (data not shown).

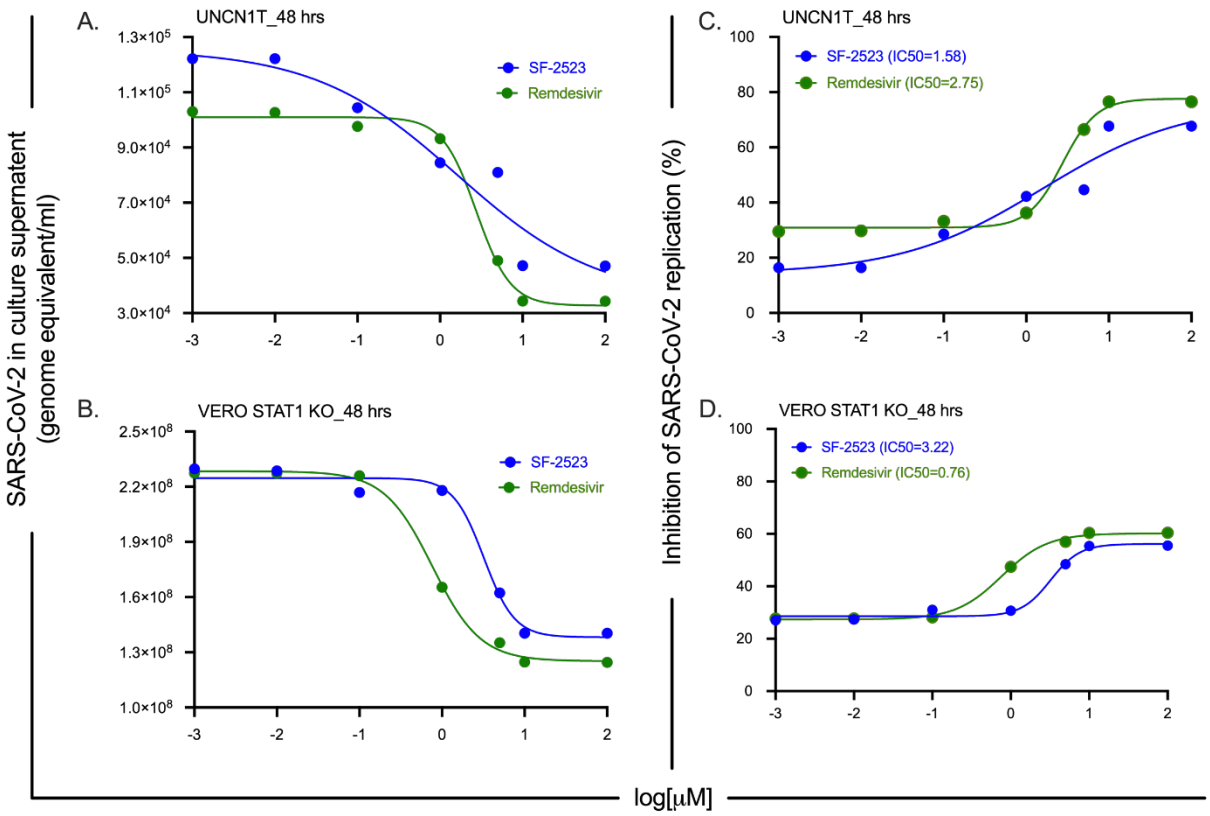

Fig S1. SARS-CoV-2 viral loads and dose-response curve in SF2523 and remdesivir treated and SARS-CoV-2 infected UNCN1T cells and Vero-STAT1 knockout cells. (**A & B**) Real-time quantitative PCR analysis of SARS-CoV-2 genome equivalent per ml of culture supernatant after 48 hrs post-infection in SF2523 (in blue) and remdesivir (in green) treated UNCN1T cells and Vero-STAT1 knockout cells with indicated drug concentrations respectively. (**C & D**) SF2523 (in blue) and remdesivir (in green) dose response curve by percentage inhibition of SARS-CoV-2 replication 48 hrs post infection in UNCN1T cells and Vero-STAT1 knockout cells with indicated drug concentrations respectively. In UNCN1T cells, SF2523 has an IC_{50} of 1.58 μM and remdesivir has an IC_{50} of 2.75 μM; In Vero-STAT1 knockout cells, SF2523 has an IC_{50} of 3.22 μM and remdesivir has an IC_{50} of 0.76 μM.

863 **Table 1: The median effective dose of individual compounds and their combination**

Vero-STAT1 knockout Cells			
Drug/Combo	**Dm**	**m**	**r**
SF2523 (S)	2.617	0.492	0.971
Remdesivir (R)	0.533	0.167	0.955
Combination (SRF)	0.452	-0.197	-0.994

UNCN1T Cells			
Drug/Combo	**Dm**	**m**	**r**
SF2523 (S)	1.836	0.222	0.953
Remdesivir (R)	0.272	0.231	0.949
Combination (SRF)	0.145	0.577	0.967

864 Dm: The median effective dose; m: The slope of the median effect (ME) plot; r: The linear correlation
865 coefficient of ME plot.

866

867 **Table 2: The CI values at different simulated effective dose of fixed dose combination of**
868 **SF2523 and remdesivir**

	CI values			
	ED50	ED75	ED90	ED95
Vero-STAT1 knockout cells	0.5105	3.75E-05	1.44E-08	7.10E-11
UNCN1T cells	0.3054	0.0173	9.91E-04	1.42E-04

869